

Role of Fe intercalation on the electronic correlation in resistively switchable antiferromagnet Fe_xNbS_2

Wenxin Li,¹ Jonathan T. Reichanadter,^{2,3,4} Shan Wu,^{3,4,5} Ji Seop Oh,^{3,6,7,8} Rourav Basak,⁹ Shannon C. Haley,³ Elio Vescovo,¹⁰ Donghui Lu,¹¹ Makoto Hashimoto,¹¹ Christoph Klewe,¹² Suchismita Sarker,¹³ Alex Frañó,⁹ James G. Analytis,^{3,14} Robert J. Birgeneau,^{3,4} Jeffrey B. Neaton,^{3,4} and Yu He^{1,*}

¹Department of Applied Physics, Yale University, New Haven, Connecticut 06511, USA

²Department of Electrical Engineering, University of California Berkeley, California, 94720, USA

³Department of Physics, University of California Berkeley, California, 94720, USA

⁴Material Sciences Division, Lawrence Berkeley National Lab, Berkeley, California, 94720, USA

⁵Department of Physics, Santa Clara University, Santa Clara, CA, 95053

⁶Department of Physics and Astronomy, Rice University, Houston, Texas 77024, USA

⁷Department of Applied Physics, Sookmyung Women's University, Seoul 04310, Republic of Korea

⁸Institute of Advanced Materials and Systems, Sookmyung Women's University, Seoul 04310, Republic of Korea

⁹Department of Physics, University of California San Diego, California, 92093, USA

¹⁰National Synchrotron Light Source II, Brookhaven National Laboratory, Upton, New York 11973, USA

¹¹Stanford Synchrotron Radiation Lightsource, SLAC National Accelerator Laboratory, Menlo Park, California 94025, USA

¹²Advanced Light Source, Lawrence Berkeley National Laboratory, Berkeley, California 94720, USA

¹³Cornell High Energy Synchrotron Source, Cornell University, Ithaca, New York 14853, USA

¹⁴CIFAR Quantum Materials, CIFAR, Toronto, Ontario M5G 1M1, Canada

(Dated: September 4, 2025)

Among the family of intercalated transition-metal dichalcogenides (TMDs), Fe_xNbS_2 is found to possess unique current-induced resistive switching behaviors, tunable antiferromagnetic states, and a commensurate charge order, all of which are tied to a critical Fe doping of $x_c = 1/3$. However, the electronic origin of such extreme stoichiometry sensitivities remains unclear. Combining angle-resolved photoemission spectroscopy (ARPES) with density functional theory (DFT) calculations, we identify and characterize a dramatic eV-scale electronic restructuring that occurs across the x_c . Moment-carrying Fe $3d_{z^2}$ electrons manifest as narrow bands within 200 meV to the Fermi level, distinct from other transition metal intercalated TMD magnets. This state strongly interacts with the itinerant electron in TMD layer, and rapidly loses coherence above x_c . These observations resemble the exceptional electronic and magnetic sensitivity of strongly correlated systems upon charge doping, shedding light on the important role of electronic correlation in magnetic TMDs.

Layered transition-metal dichalcogenides (TMD) TA_2 ($\text{T} = \text{Ta}, \text{Nb}, \text{Mo}$; $\text{A} = \text{Se}, \text{S}$) constitute a family of materials that are pivotal to modern condensed matter physics research, owing to their diverse physical properties and versatile applications, ranging from charge density wave to superconductivity [1–4]. While most TMDs assume a weakly correlated non-magnetic ground state in their pristine phase [5, 6], their layered crystal structure often allows for $3d$ transition metal ion intercalants to populate the van der Waals (vdW) gap (M_xTA_2 , $\text{M} = 3d$ transition metal). This leads to a versatile class of tunable layered magnets that are often also highly metallic [7, 8], where indirect exchange via itinerant electrons is considered indispensable given the large M-site distances. Among all possible intercalant concentrations, materials with intercalation ratio $x_c = 1/3$, where the intercalated atoms typically form into a $\sqrt{3} \times \sqrt{3}$ superlattice [9] with non-centrosymmetric space group $P6_322$ and a folded Brillouin zone (Figure 1 (a)(b)) have drawn considerable interest with their extensive display of diverse magnetic and electronic properties [10–18].

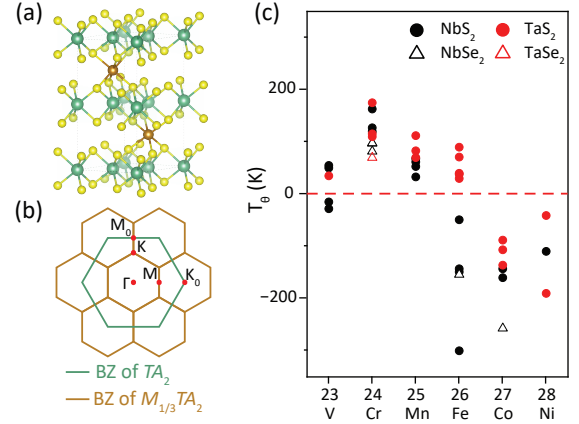


FIG. 1. Structural and magnetic property of intercalated TMD magnets. (a) The crystallographic structure and (b) Brillouin zone of $3d$ metal intercalated TMDs M_xTA_2 with $x = 1/3$. (c) Compilation of the Curie-Weiss temperatures for various M_xTA_2 systems [7, 16, 19–35].

Figure 1 (c) tallies the Curie-Weiss temperature T_θ for different M_xTA_2 materials with highly tunable magnetic correlations [7, 16, 19–35]. Except for $\text{V}_{1/3}\text{NbS}_2$,

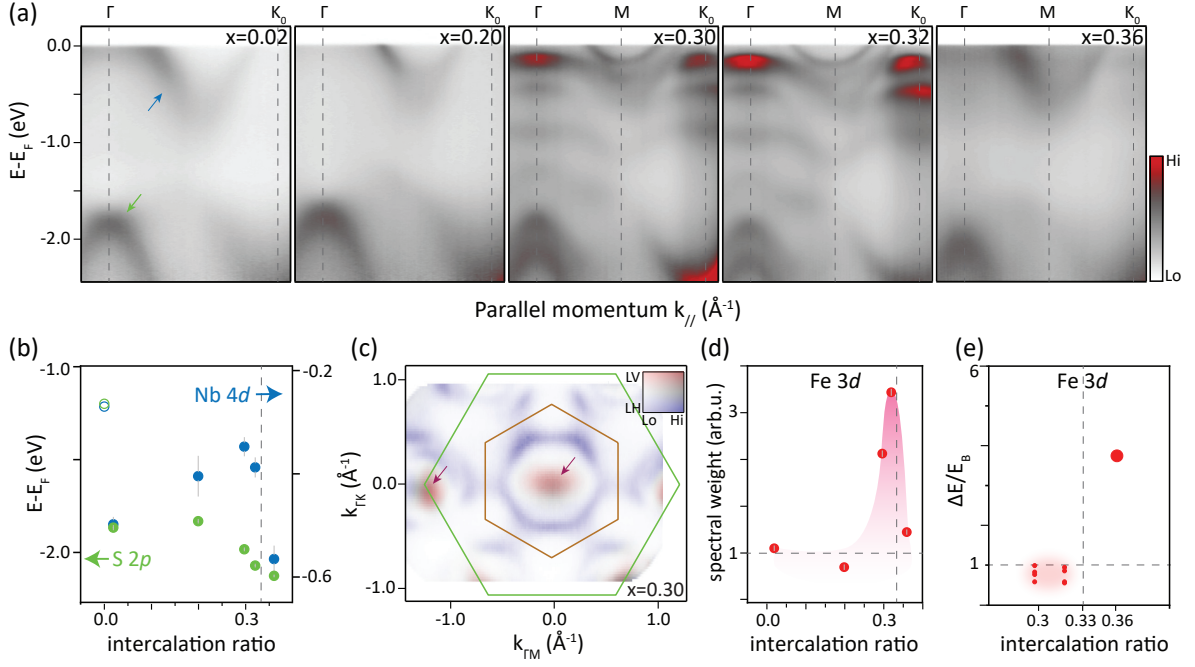


FIG. 2. ARPES measurement of Fe_xNbS_2 across different Fe stoichiometry. (a) Energy-momentum cut along Γ -M- K_0 with different Fe stoichiometry. (b) Evolution of the position of S 2p and Nb 4d derived bands with increasing Fe stoichiometry. Data for $x = 0$ (hollow points) are extracted from [36]. (c) Constant energy contours integrated between $E_B = 0.2$ eV and 0.1 eV for $x = 0.30$. Purple arrows indicate Fe-derived bands. (d) Evolution of spectral weight of the Fe-derived bands with increasing Fe stoichiometry. Spectral weight integrated between $[0,1]$ eV binding energy and $\pm 0.2 \text{ \AA}^{-1}$ of Γ . (e) Evolution of full width at half maximum (FWHM) divided by binding energy of quasiparticle peaks with increasing Fe stoichiometry extracted from the energy distribution curves (EDC) at Γ .

which has a controversial magnetic ground state and was recently proposed as an altermagnet [37, 38], Fe intercalation is uniquely associated with both ferromagnetic and antiferromagnetic correlations depending on the TMD layers. This implies an active role of the TMD layer in mediating long-range Fe-Fe magnetic exchange, and makes Fe-intercalated TA_2 materials hosts for highly tunable magnetism and magnetoelectric transport properties. Recent neutron scattering measurements reported two distinct magnetic phases across $x_c = 1/3$, i.e., the antiferromagnetic stripe order at $k_{m1} = (0.5, 0, 0)$ for $x < x_c$, and the antiferromagnetic zigzag order at $k_{m2} = (0.25, 0.5, 0)$ for $x > x_c$ [39]. These highly tunable magnetic phases in Fe_xNbS_2 are believed to relate to its current-induced resistance switching property, which changes sign across x_c [40–42]. Moreover, a commensurate three-dimensional charge order, concomitant with the magnetic ordering, was recently discovered for $x > x_c$, signaling strongly coupled charge and magnetic degrees of freedom [43].

It remains a mystery why both the electrical transport and magnetic ordering properties experience a sudden change across $x_c = 1/3$ in and only in Fe_xNbS_2 . Previous electronic structure investigations in various intercalated TMD systems show that the low-energy

electronic structure mainly derives from the TMD layers, while the charge doping and minor band hybridization effects come from the intercalated 3d transition metal [44–52]. However, the extreme sensitivities around x_c in the Fe-intercalated system, akin to those in strongly correlated electron systems, motivate systematic electronic and structural investigations into what makes Fe intercalants special. In this work, we combine angle-resolved photoemission spectroscopy (ARPES), X-ray photoelectron spectroscopy (XPS), single crystal X-ray diffraction (XRD), X-ray absorption spectroscopy (XAS) and density functional theory (DFT) calculations to investigate the electronic structure of Fe_xNbS_2 near the critical doping x_c , with a specific focus on the roles of itinerant and local electrons.

Given the extreme surface sensitivity of photoemission experiments [53, 54] and the existence of inhomogeneous surface termination in other intercalated TMD systems [49, 50], micro-spot XPS measurements are performed on *in-situ* cleaved bulk sample surfaces to examine the iron homogeneity. Compared to the micron-scale inhomogeneity reported in $\text{V}_{1/3}\text{NbS}_2$ [50] and $\text{Cr}_{1/3}\text{NbS}_2$ [49], the surface iron inhomogeneity here can be constrained to less than 2.8% over similar length scales (see Supplementary Information (SI) [55]), enabling intrinsic electronic structure investigation as

the bulk doping is tuned across $x_c = 1/3$. Figure 2 (a) shows the electronic structure measured with ARPES along the direction Γ - K_0 from $x = 0.02$ to $x = 0.36$. For doping close to x_c , the $\sqrt{3} \times \sqrt{3}$ Fe-superlattice forms (see SI [55]) so that the M point of the Brillouin zone of $\text{Fe}_{1/3}\text{NbS}_2$ lies in the middle of Γ and K_0 points.

We first investigate the charge doping effect introduced by Fe intercalation. By tracking the energy positions of the band extrema for the Nb 4d and the S 2p bands, Fig. 2 (b) shows that Fe intercalants only act as a simple charge donor at very dilute doping ($x=0.02$) as expected in doped semiconductors [7, 44]. Further iron intercalation causes this charge transfer process to reverse course, where the Nb 4d bands are gradually depleted (rising band bottom), pointing to potential electron localization at the Fe sites. Only when doped to $x > x_c$, electrons move to fill Nb 4d bands again. On the other hand, S 2p bands shift toward higher binding energy during Fe intercalation, indicating a globally increasing chemical potential. This suggests reversed charge flow from Nb 4d states to Fe 3d states as the system approaches x_c .

This anomalous charge transfer behavior naturally raises the question of where the extra Fe 3d electrons go, which are supposed to carry magnetic moments. Strikingly, at $x = 0.30$ and $x = 0.32$ where Nb states receive the least charge doping, a cascade of weakly dispersive Fe 3d bands forms at Γ , with in-plane bandwidths less than 150 meV. These states are notably absent in other 3d transition metal intercalated TMDs reported to date. Figure 2 (c) shows the momentum-dependent spectral intensity integrated between $E_B = 0.1$ eV and 0.2 eV where the Fe 3d bands are primarily located. Here, orbital contributions reflected through orthogonal incident photon polarizations are color-coded in red and blue [56]. Via photoemission matrix element analysis, these low-energy narrow bands are mainly of $3d_{z^2}$ orbital character [57], and are found to repeat corresponding to the Fe-sublattice Brillouin zone. They belong to the t_{2g} states in the Fe ion's local symmetry coordinate basis, consistent with our magnetic DFT calculations (see SI [55]), and are expected to carry local magnetic moments despite their very low binding energy of less than 1 eV — a stark contrast to what is typically observed in other 3d metal-intercalated TMDs [58, 59]. This not only offers a natural explanation for the “missing electrons” that would have delocalized into the TMD layers, but also hints at the associated sensitivity for magnetism against low-energy chemical, electrical, and temperature tuning.

Given that d_{z^2} orbital is expected to extend along c axis and be the primary orbital to bridge adjacent NbS_2 layers, we turn to investigate whether these

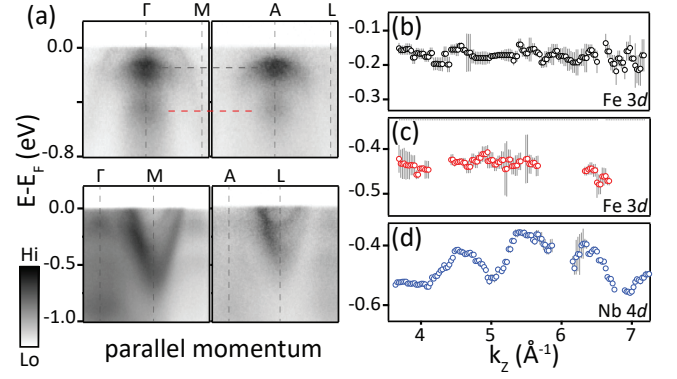


FIG. 3. Mixed dimensionality shown from ARPES measurement. (a) Energy-momentum cut along Γ - M - K_0 and A - L - H_0 for $x = 0.30$ collected at LV (upper panel) and LH (lower panel) polarizations, respectively. The black and red dash lines are visual guides to compare band energy positions. (b) (c) Fitted result showing k_z dispersion for Fe-derived bands (black and red circles) and Nb-derived bands (blue circles).

electrons facilitate c axis itineracy or are sufficiently localized to contribute to local moments. Figure 3 shows the energy-momentum cut along Γ - M and A - L directions, as well as the k_z dispersion for Fe 3d and Nb 4d bands. Here, the Fe $3d_{z^2}$ bands show negligible k_z dispersion (Fig. 3(b)(c)), confirming the localized nature of low-energy Fe states along all directions. In contrast, the Nb 4d band gains substantial k_z dispersion on the order of ~ 200 meV compared to mere ~ 35 meV in undoped NbS_2 [36]. This observation reveals the sophisticated role of the Fe intercalant in these systems: providing c axis conduction pathways for NbS_2 electrons, while holding onto its own electrons to carry local moments. Meanwhile, Nb 4d electrons receive a massive c -axis hopping enhancement across the vdW gap through the intercalated iron. This makes it possible to achieve robust, meV scale effective exchange for both in-plane and out-of-plane Fe near neighbors via long-range RKKY interactions [60–62], consistent with previous neutron scattering experiment and magnetic DFT calculations [39]. This is also distinct from the idealized 2D nature of pristine TMD systems [2, 4, 36], and adds nuance to the common notion of intercalated TMDs as prototype 2D magnets [7, 8, 19, 21, 26, 34].

To understand the acute doping dependence of charge, magnetic, and transport properties across x_c , we now turn to the doping dependent electronic structure. Surprisingly, the low-energy Fe 3d states suddenly lose spectral weight above x_c (Fig. 2 (a) and (d), see also SI for spectral normalization procedures [55]). If quasiparticles are considered well defined when their energy widths are smaller than their binding energy ($\Delta E/E_B < 1$), low-energy Fe 3d quasiparticles vanish

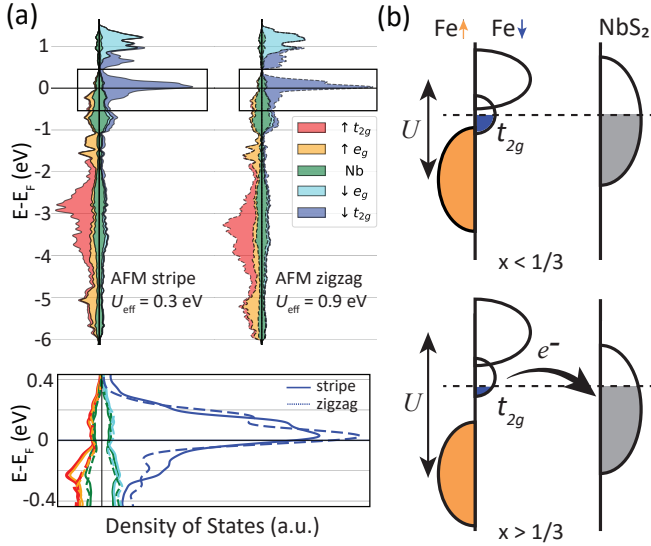


FIG. 4. (a) Projected electronic density of states (DOS) of the Fe spin sublattices in $\text{Fe}_{1/3}\text{NbS}_2$ for AFM stripe (left) and AFM zigzag (right) magnetic phases as computed by DFT. The Fe 3d orbitals are further projected by their t_{2g} and e_g irreducible representation characters as well as their spin channels of spin-up (bonding) and spin-down (anti-bonding) respectively (indicated by different colors). (b) Orbital diagrams depicting the Fe 3d band splitting and occupation below and above the critical doping boundary $x_c = 1/3$.

above x_c (Fig. 2 (e), see SI for detailed analysis [55]). Fe site-disorder effect is minimal and smoothly evolves across x_c shown by high-resolution synchrotron XRD (see SI [55]). Meanwhile, surface termination inhomogeneity is ruled out by both micro-XPS analysis at micron-scale and the robust observation of the same phenomena over a wide range of photon energies, as illustrated in Figure 3 and SI [55]. Notably, no discernible Fermi surface folding is seen with the cascade of magnetic and charge orders, ruling out simple low-energy Fermi surface nesting scenarios (see SI [55]) [43]. These observations all point to the possible involvement of strong correlation behind this sudden change in electronic structure across x_c , reminiscent of recent discoveries in cuprate high-temperature superconductors, where a sudden loss of quasiparticle coherence occurs across a critical doping [63–65], as well as in Fe-based superconductors, where a coherent-to-incoherent crossover happens when the Fe $3d_{xy}$ orbital becomes weakly localized [66, 67]. To understand the nature of the localized low-energy bands observed with ARPES, we perform spin-polarized DFT calculations for stoichiometric $\text{Fe}_{1/3}\text{NbS}_2$ with the generalized gradient approximation of Perdew, Burke, and Ernzerhof (PBE) functional [68] and a Hubbard U correction [69] acting on the Fe d electrons. The Vienna Ab initio simulation package (VASP) [70] is used for all calculations; further computational details are provided in SI [55]. Following prior calculations on

$\text{Fe}_{1/3}\text{NbS}_2$ [39, 71], we employ a U of 0.3 eV for the AFM stripe phase ($x < x_c$) and 0.9 eV ($x > x_c$) for the AFM zigzag phase. These computational choices lead to computed magnetic moments on the Fe sites of 2.86 and 2.89 μ_B for stripe and zigzag phases, respectively, in agreement with prior reports [30, 39, 72].

Figure 4 (a) plots the computed partial density of states (PDOS) for one of the Fe spin sublattices in the stripe (zigzag) antiferromagnetic phase in the left (right) sub-panel with Nb-projected states overlaid. The pseudo-octahedral coordination localized about each Fe cation motivates projecting the PDOS onto t_{2g} and e_g 3d molecular orbitals (see SI [55] for details), which reveals that the strong peak in the DOS near the Fermi level is dominantly of Fe 3d t_{2g} character. This finding corroborates the earlier interpretation of ARPES data near x_c in Figure 2 (a) where non-dispersive band features are attributed to Fe $3d_{z^2}$ states. The full occupation of the Fe 3d e_g bonding orbitals and the partial filling of the Fe 3d anti-bonding t_{2g} orbitals support a high-spin Fe(II) oxidation state consistent with our calculations and prior neutron scattering studies [39]. Further, the bonding Fe e_g 3d states below the Fermi energy divide into two broad levels separated by a ~ 2 eV interval. This subsequent splitting of the occupied e_g level is evidence of a crystal field associated with the Fe site’s lower C_{3v} global point group symmetry [73] and reflects significant hybridization of the Fe and Nb states. Strong Fe-Nb hybridization is relevant to the proposed RKKY coupling between Fe spins [39, 71] and invites further investigation into possible Kondo-like interactions between the localized Fe 3d states and itinerant NbS₂ states [60, 62, 74–77]. This hybridization is evident from the greater broadening of the occupied compared to the unoccupied Fe 3d states, and from their energy overlap with the occupied Nb 4d states in the Nb-projected PDOS shown in Fig. 4(a).

Notably, the partially-occupied t_{2g} states residing at the Fermi energy (E_F) differ for the two phases, with substantial reorganization of these antibonding 3d states in the zigzag phase relative to stripe. As shown in the zoomed-in view between -400 meV and 400 meV of the PDOS plot in Figure 4 (a), in the transition from the stripe to the zigzag phase, this t_{2g} level is globally pushed above E_F , while the PDOS tail below E_F spreads across the [0,400] meV binding energy, consistent with the quasiparticle decoherence observed in ARPES for $x > x_c$ (Figure 2). More drastic differences in the PDOS of the occupied t_{2g} orbitals further below E_F between the two phases are also observed in our calculations. The schematic in Figure 4 (b) summarizes the electronic structure evolution across x_c . As x increases above $1/3$, the zigzag phase is favored, where the increasing U depopulates these t_{2g} states and causes a decoherence of

occupied Fe states above x_c , leading to more electrons returning to the Nb $4d$ states. This scenario is consistent with the observation in Fig. 2 (a)(b), as well as a slightly enhanced Fe pre- L_3 edge peak for $x = 0.36$ in XAS measurements (see SI [55]) and the slightly increased ordered moment size due to the removal of anti-bonding Fe electrons for $x > x_c$ seen in neutron scattering [39]. Although the microscopic origin of the enhanced correlation effect above x_c still calls for further experimental and theoretical investigations, it is plausible that this enhanced correlation effect could be the cause of the rapid decoherence of Fe states across x_c , as well as the sudden change of the magnetic ground state that leads to opposite resistive switching behavior [71].

Our work suggests that Fe intercalated TMD is a unique correlated electron system, where the moment-carrying narrow-bandwidth Fe $3d_{z^2}$ states are within 0.2 eV below E_F , and are extremely sensitive to intercalation-tuned correlation effects. The proximity of Fe $3d_{z^2}$ state to E_F , unique among other M_xTA_2 systems, also helps understand the abrupt changes across $x_c = 1/3$ absent in other intercalated TMD systems. Finally, atomically resolved probes, such as scanning tunneling microscope/spectroscopy (STM/S) may help shed light on the microscopic origin of the sudden change in the correlation strength in Fe across x_c , possibly by revealing local Fe vacancy or interstitial disorders and the corresponding local density of states (DOS).

ACKNOWLEDGMENTS

We thank Eduardo H. da Silva Neto, Pranab Kumar-Nag, Xinze Yang, Sophie Weber, and Ruihua He for helpful discussions. The photoemission and x-ray diffraction works are funded by the U.S. Air Force Office of Scientific Research under Award No. FA9550-24-1-0048. W. L. acknowledges support from James Kouvel Fellowship. Work at the University of California, Berkeley and Lawrence Berkeley National Laboratory was funded by the U.S. DOE, Office of Science, Office of Basic Energy Sciences, Materials Sciences and Engineering Division under Contract No. DE-AC02-05CH11231 (Quantum Materials Program KC2202). Work at the University of California, San Diego was supported by the National Science Foundation under Grant No. DMR-2145080. Bulk crystal growth of NbS₂ materials was supported by the 2DCC-MIP under NSF cooperative agreement DMR-2039351. Use of the Stanford Synchrotron Radiation Lightsource, SLAC National Accelerator Laboratory, is supported by the U.S. Department of Energy, Office of Science, Office of Basic Energy Sciences under Contract No. DE-AC02-76SF00515. This research used resources of the National Synchrotron Light Source

II, a U.S. Department of Energy (DOE) Office of Science User Facility operated for the DOE Office of Science by Brookhaven National Laboratory under Contract No. DE-SC0012704. We acknowledge Yale West Campus Materials Characterization Core. This work is based on research conducted at the Center for High-Energy X-ray Sciences (CHEXS), which is supported by the National Science Foundation (BIO, ENG and MPS Directorates) under award DMR-2342336. This research used resources of the Advanced Light Source, a US DOE Office of Science User Facility under Contract No. DE-AC02-05CH11231.

* yu.he@yale.edu

- [1] J. Wilson, F. D. Salvo, and S. Mahajan, Charge-density waves and superlattices in the metallic layered transition metal dichalcogenides, *Advances in Physics* **24**, 117 (1975).
- [2] S. V. Borisenko, A. A. Kordyuk, V. B. Zabolotnyy, D. S. Inosov, D. Evtushinsky, B. Büchner, A. N. Yaresko, A. Varykhalov, R. Follath, W. Eberhardt, L. Patthey, and H. Berger, Two energy gaps and fermi-surface “arcs” in nbse₂, *Phys. Rev. Lett.* **102**, 166402 (2009).
- [3] T. Valla, A. V. Fedorov, P. D. Johnson, P.-A. Glans, C. McGuinness, K. E. Smith, E. Y. Andrei, and H. Berger, Quasiparticle spectra, charge-density waves, superconductivity, and electron-phonon coupling in 2H-nbse₂, *Phys. Rev. Lett.* **92**, 086401 (2004).
- [4] D. J. Rahn, S. Hellmann, M. Kalläne, C. Sohrt, T. K. Kim, L. Kipp, and K. Rossnagel, Gaps and kinks in the electronic structure of the superconductor 2h-nbse₂ from angle-resolved photoemission at 1 k, *Phys. Rev. B* **85**, 224532 (2012).
- [5] S. Manzeli, D. Ovchinnikov, D. Pasquier, O. V. Yazyev, and A. Kis, 2d transition metal dichalcogenides, *Nature Reviews Materials* **2**, 17033 (2017).
- [6] W. Choi, N. Choudhary, G. H. Han, J. Park, D. Akinwande, and Y. H. Lee, Recent development of two-dimensional transition metal dichalcogenides and their applications, *Materials Today* **20**, 116 (2017).
- [7] S. S. P. Parkin and R. H. Friend, 3d transition-metal intercalates of the niobium and tantalum dichalcogenides. i. magnetic properties, *Philosophical Magazine B* **41**, 65 (1980).
- [8] R. H. Friend, A. R. Beal, and A. D. Yoffe, Electrical and magnetic properties of some first row transition metal intercalates of niobium disulphide, *The Philosophical Magazine: A Journal of Theoretical Experimental and Applied Physics* **35**, 1269 (1977).
- [9] F. Boswell, A. Prodan, W. R. Vaughan, and J. Corbett, On the ordering of Fe atoms in FexNbS₂, physics status solidi (a) **45** (1978).
- [10] Y. Togawa, T. Koyama, K. Takayanagi, S. Mori, Y. Kousaka, J. Akimitsu, S. Nishihara, K. Inoue, A. S. Ovchinnikov, and J. Kishine, Chiral magnetic soliton lattice on a chiral helimagnet, *Phys. Rev. Lett.* **108**, 107202 (2012).
- [11] D. Braam, C. Gomez, S. Tezok, E. V. L. de Mello, L. Li, D. Mandrus, H.-Y. Kee, and J. E. Sonier, Magnetic

- properties of the helimagnet $\text{Cr}_{1/3}\text{NbS}_2$ observed by μSR , *Phys. Rev. B* **91**, 144407 (2015).
- [12] Y. Kousaka, T. Ogura, J. Zhang, P. Miao, S. Lee, S. Torii, T. Kamiyama, J. Campo, K. Inoue, and J. Akimitsu, Long periodic helimagnetic ordering in CrM_3S_6 ($m = \text{Nb}$ and Ta), *Journal of Physics: Conference Series* **746**, 012061 (2016).
 - [13] Y. Kousaka, Y. Nakao, J. Kishine, M. Akita, K. Inoue, and J. Akimitsu, Chiral helimagnetism in $\text{tI}/3\text{NbS}_2$ ($t = \text{Cr}$ and Mn), *Nuclear Instruments and Methods in Physics Research Section A: Accelerators, Spectrometers, Detectors and Associated Equipment* **600**, 250 (2009).
 - [14] S. K. Karna, F. N. Womack, R. Chapai, D. P. Young, M. Marshall, W. Xie, D. Graf, Y. Wu, H. Cao, L. DeBeer-Schmitt, P. W. Adams, R. Jin, and J. F. DiTusa, Consequences of magnetic ordering in chiral $\text{Mn}_{1/3}\text{NbS}_2$, *Phys. Rev. B* **100**, 184413 (2019).
 - [15] Y. Togawa, T. Koyama, Y. Nishimori, Y. Matsumoto, S. McVitie, D. McGrouther, R. L. Stamps, Y. Kousaka, J. Akimitsu, S. Nishihara, K. Inoue, I. G. Bostrem, V. E. Sinitsyn, A. S. Ovchinnikov, and J. Kishine, Magnetic soliton confinement and discretization effects arising from macroscopic coherence in a chiral spin soliton lattice, *Phys. Rev. B* **92**, 220412 (2015).
 - [16] N. J. Ghimire, A. S. Botana, J. S. Jiang, J. Zhang, Y. S. Chen, and J. F. Mitchell, Large anomalous hall effect in the chiral-lattice antiferromagnet CoNb_3S_6 , *Nature Communications* **9**, 3280 (2018).
 - [17] R. Aoki, Y. Kousaka, and Y. Togawa, Anomalous nonreciprocal electrical transport on chiral magnetic order, *Phys. Rev. Lett.* **122**, 057206 (2019).
 - [18] P. Park, Y.-G. Kang, J. Kim, K. H. Lee, H.-J. Noh, M. J. Han, and J.-G. Park, Field-tunable toroidal moment and anomalous hall effect in noncollinear antiferromagnetic Weyl semimetal $\text{Co}_1/3\text{TaS}_2$, *npj Quantum Materials* **7**, 42 (2022).
 - [19] J. van den Berg and P. Cossee, Structural aspects and magnetic behaviour of NbS_2 and TaS_2 containing extra metal atoms of the first transition series, *Inorganica Chimica Acta* **2**, 143 (1968).
 - [20] F. Hulliger and E. Pobitschka, On the magnetic behavior of new $2\text{H}-\text{NbS}_2$ -type derivatives, *Journal of Solid State Chemistry* **1**, 117 (1970).
 - [21] B. Van Laar, H. Rietveld, and D. Ijdo, Magnetic and crystallographic structures of Me_xNbS_2 and Me_xTaS_2 , *Journal of Solid State Chemistry* **3**, 154 (1971).
 - [22] M. Eibschütz, F. J. DiSalvo, J. Hull, G. W., and S. Mahajan, Ferromagnetism in metallic Fe_xTaS_2 ($x \approx 0.28$), *Applied Physics Letters* **27**, 464 (1975).
 - [23] A. L. Blanc-Soreau, J. Rouxel, M.-F. Gardette, and O. Gorochoff, Propriétés électriques et magnétiques de $\text{Mn}_{0.25}\text{NbS}_2$ et $\text{Mn}_{0.33}\text{NbS}_2$, *Materials Research Bulletin* **11**, 1061 (1976).
 - [24] H. Wang, X.-P. Ma, X.-Y. Zeng, J. Gong, J.-F. Lin, X.-Y. Wang, Z.-Y. Dai, K. Han, Y.-T. Wang, and T.-L. Xia, Anomalous hall effect and topological hall effect in the noncollinear antiferromagnet $\text{V}_{0.3}\text{NbS}_2$, *Phys. Rev. B* **107**, 134436 (2023).
 - [25] T. Inoshita, M. Hirayama, N. Hamada, H. Hosono, and S. Murakami, Topological semimetal phases manifested in transition metal dichalcogenides intercalated with $3d$ metals, *Phys. Rev. B* **100**, 121112 (2019).
 - [26] Y. Yamasaki, R. Moriya, M. Arai, S. Masubuchi, S. Pyon, T. Tamegai, K. Ueno, and T. Machida, Exfoliation and van der Waals heterostructure assembly of intercalated ferromagnet $\text{Cr}_1/3\text{TaS}_2$, *2D Materials* **4**, 041007 (2017).
 - [27] A. F. Gubkin, E. P. Proskurina, Y. Kousaka, E. M. Sherokalova, N. V. Selezneva, P. Miao, S. Lee, J. Zhang, Y. Ishikawa, S. Torii, T. Kamiyama, J. Campo, J. Akimitsu, and N. V. Baranov, Crystal and magnetic structures of $\text{Cr}_1/3\text{NbS}_2$ from neutron diffraction, *Journal of Applied Physics* **119**, 013903 (2016).
 - [28] N. Toporova, E. Sherokalova, N. Selezneva, V. Ogloblichev, and N. Baranov, Crystal structure, properties and Griffiths-like phase in niobium diselenide intercalated with chromium, *Journal of Alloys and Compounds* **848**, 156534 (2020).
 - [29] H. Zhang, W. Wei, G. Zheng, J. Lu, M. Wu, X. Zhu, J. Tang, W. Ning, Y. Han, L. Ling, J. Yang, W. Gao, Y. Qin, and M. Tian, Electrical and anisotropic magnetic properties in layered $\text{Mn}_1/3\text{TaS}_2$ crystals, *Applied Physics Letters* **113**, 072402 (2018).
 - [30] P. Liu, H. Zhu, Q. Wu, Y. Lu, and Y. Pu, Unconventional magneto-transport properties of the layered antiferromagnet $\text{Fe}_1/3\text{NbS}_2$, *Applied Physics Letters* **121**, 081901 (2022).
 - [31] S. Mangelsen, J. Hansen, P. Adler, W. Schnelle, W. Bensch, S. Mankovsky, S. Polesya, and H. Ebert, Large anomalous hall effect and slow relaxation of the magnetization in $\text{Fe}_1/3\text{TaS}_2$, *The Journal of Physical Chemistry C* **124**, 24984 (2020).
 - [32] J. Dijkstra, P. J. Zijlema, C. F. van Bruggen, C. Haas, and R. A. de Groot, Band-structure calculations of $\text{Fe}_1/3\text{TaS}_2$ and $\text{Mn}_1/3\text{TaS}_2$, and transport and magnetic properties of $\text{Fe}_{0.28}\text{TaS}_2$, *Journal of Physics: Condensed Matter* **1**, 6363 (1989).
 - [33] K. Lu, A. Murzabekova, S. Shim, J. Park, S. Kim, L. Kish, Y. Wu, L. DeBeer-Schmitt, A. A. Aczel, A. Schleife, N. Mason, F. Mahmood, and G. J. MacDougall, Understanding the anomalous hall effect in $\text{Co}_1/3\text{NbS}_2$ from crystal and magnetic structures (2022), [arXiv:2212.14762](https://arxiv.org/abs/2212.14762).
 - [34] Y. Liu, Z. Hu, X. Tong, E. D. Bauer, and C. Petrovic, Electrical and thermal transport in van der Waals magnets $2\text{H}-\text{M}_x\text{TaS}_2$ ($\text{M} = \text{Mn}, \text{Co}$), *Phys. Rev. Res.* **4**, 013048 (2022).
 - [35] Y. An, P. Park, C. Kim, K. Zhang, H. Kim, M. Avdeev, J. Kim, M.-J. Han, H.-J. Noh, S. Seong, J.-S. Kang, H.-D. Kim, and J.-G. Park, Bulk properties of the chiral metallic triangular antiferromagnets $\text{Ni}_{1/3}\text{NbS}_2$ and $\text{Ni}_{1/3}\text{TaS}_2$, *Phys. Rev. B* **108**, 054418 (2023).
 - [36] Z. El Youbi, S. W. Jung, C. Richter, K. Hricovini, C. Cacho, and M. D. Watson, Fermiology and electron-phonon coupling in the 2H and 3R polytypes of NbS_2 , *Phys. Rev. B* **103**, 155105 (2021).
 - [37] L. Šmejkal, J. Sinova, and T. Jungwirth, Beyond conventional ferromagnetism and antiferromagnetism: A phase with nonrelativistic spin and crystal rotation symmetry, *Phys. Rev. X* **12**, 031042 (2022).
 - [38] L. Šmejkal, J. Sinova, and T. Jungwirth, Emerging research landscape of altermagnetism, *Phys. Rev. X* **12**, 040501 (2022).
 - [39] S. Wu, Z. Xu, S. C. Haley, S. F. Weber, A. Acharya, E. Maniv, Y. Qiu, A. A. Aczel, N. S. Settineri, J. B. Neaton, J. G. Analytis, and R. J. Birgeneau, Highly tunable magnetic phases in transition-metal dichalcogenide $\text{Fe}_{1/3+\delta}\text{NbS}_2$, *Phys. Rev. X* **12**, 021003 (2022).

- [40] N. L. Nair, E. Maniv, C. John, S. Doyle, J. Orenstein, and J. G. Analytis, Electrical switching in a magnetically intercalated transition metal dichalcogenide, *Nature Materials* **19**, 153 (2020).
- [41] E. Maniv, R. A. Murphy, S. C. Haley, S. Doyle, C. John, A. Maniv, S. K. Ramakrishna, Y.-L. Tang, P. Ercius, R. Ramesh, A. P. Reyes, J. R. Long, and J. G. Analytis, Exchange bias due to coupling between coexisting antiferromagnetic and spin-glass orders, *Nature Physics* **10.1038/s41567-020-01123-w** (2021).
- [42] E. Maniv, N. L. Nair, S. C. Haley, S. Doyle, C. John, S. Cabrini, A. Maniv, S. K. Ramakrishna, Y.-L. Tang, P. Ercius, R. Ramesh, Y. Tserkovnyak, A. P. Reyes, and J. G. Analytis, Antiferromagnetic switching driven by the collective dynamics of a coexisting spin glass, *Science Advances* **7**, 10.1126/sciadv.abd8452 (2021).
- [43] S. Wu, R. Basak, W. Li, J.-W. Kim, P. J. Ryan, D. Lu, M. Hashimoto, C. Nelson, R. Acevedo-Estevés, S. C. Haley, J. G. Analytis, Y. He, A. Frano, and R. J. Birgeneau, Discovery of charge order in the transition metal dichalcogenide $\text{Fe}_{1/3}\text{NbS}_2$, *Phys. Rev. Lett.* **131**, 186701 (2023).
- [44] Z. Hawkhead, T. J. Hicken, N. P. Bentley, B. M. Huddart, S. J. Clark, and T. Lancaster, Band-filling-controlled magnetism from transition metal intercalation in $\text{N}_{1/3}\text{NbS}_2$ revealed with first-principles calculations, *Phys. Rev. Mater.* **7**, 114002 (2023).
- [45] C. Battaglia, H. Cercellier, L. Despont, C. Monney, M. Prester, H. Berger, L. Forró, M. G. Garnier, and P. Aebi, Non-uniform doping across the fermi surface of nbs_2 intercalates, *The European Physical Journal B* **57**, 385 (2007).
- [46] P. Popčević, Y. Utsumi, I. Biało, W. Tabis, M. A. Gala, M. Rosmus, J. J. Kolodziej, N. Tomaszewska, M. Garb, H. Berger, I. Batistić, N. Barišić, L. Forró, and E. Tutiš, Role of intercalated cobalt in the electronic structure of $\text{Co}_{1/3}\text{NbS}_2$, *Phys. Rev. B* **105**, 155114 (2022).
- [47] N. Qin, C. Chen, S. Du, X. Du, X. Zhang, Z. Yin, J. Zhou, R. Xu, X. Gu, Q. Zhang, W. Zhao, Y. Li, S.-K. Mo, Z. Liu, S. Zhang, Y. Guo, P. Tang, Y. Chen, and L. Yang, Persistent exchange splitting in the chiral helimagnet $\text{Cr}_{1/3}\text{NbS}_2$, *Phys. Rev. B* **106**, 035129 (2022).
- [48] N. Sirica, S.-K. Mo, F. Bondino, I. Pis, S. Nappini, P. Vilmercati, J. Yi, Z. Gai, P. C. Snijders, P. K. Das, I. Vobornik, N. Ghimire, M. R. Koehler, L. Li, D. Sapkota, D. S. Parker, D. G. Mandrus, and N. Mannella, Electronic structure of the chiral helimagnet and 3d-intercalated transition metal dichalcogenide $\text{Cr}_{1/3}\text{NbS}_2$, *Phys. Rev. B* **94**, 075141 (2016).
- [49] L. S. Xie, O. Gonzalez, K. Li, M. Michiardi, S. Gorovikov, S. H. Ryu, S. S. Fender, M. Zonno, N. H. Jo, S. Zhdanovich, C. Jozwiak, A. Bostwick, S. Husremović, M. P. Erodici, C. Mollazadeh, A. Damascelli, E. Rotenberg, Y. Ping, and D. K. Bediako, Comparative electronic structures of the chiral helimagnets $\text{Cr}_{1/3}\text{NbS}_2$ and $\text{Cr}_{1/3}\text{TaS}_2$, *Chemistry of Materials* **35**, 7239 (2023).
- [50] B. Edwards, O. Dowinton, A. E. Hall, P. A. E. Murgatroyd, S. Buchberger, T. Antonelli, G.-R. Siemann, A. Rajan, E. A. Morales, A. Zivanovic, C. Bigi, R. V. Belosludov, C. M. Polley, D. Carbone, D. A. Mayoh, G. Balakrishnan, M. S. Bahramy, and P. D. C. King, Giant valley-zeeman coupling in the surface layer of an intercalated transition metal dichalcogenide, *Nature Materials* **22**, 459 (2023).
- [51] Y. U. Boucher, I. Biało, M. A. Gala, W. Tabis, M. Rosmus, N. Olszowska, J. J. Kolodziej, B. Gudac, M. Novak, N. K. C. Muniraju, I. Batistić, N. Barišić, P. Popčević, and E. Tutiš, Intercalation-induced states at the fermi level and the coupling of intercalated magnetic ions to conducting layers in $\text{Ni}_{1/3}\text{NbS}_2$ (2024), [arXiv:2401.05884](https://arxiv.org/abs/2401.05884) [cond-mat.mtrl-sci].
- [52] A. Kar, R. Basak, X. Li, A. Korshunov, D. Subires, J. Phillips, C. Y. Lim, F. Zhou, L. Song, W. Wang, Y.-C. Lau, G. Garbarino, P. Gargiani, Y. Zhao, C. Plueckthun, S. Francoual, A. Jana, I. Vobornik, T. Valla, A. Rajapitamahuni, J. G. Analytis, R. J. Birgeneau, E. Vescovo, A. Bosak, J. Dai, M. Tallarida, A. Frano, V. Pardo, S. Wu, and S. Blanco-Canosa, Magnetoelastic coupling in intercalated transition metal dichalcogenides (2025), [arXiv:2503.14444](https://arxiv.org/abs/2503.14444) [cond-mat.str-el].
- [53] A. Damascelli, Z. Hussain, and Z.-X. Shen, Angle-resolved photoemission studies of the cuprate superconductors, *Rev. Mod. Phys.* **75**, 473 (2003).
- [54] J. A. Sobota, Y. He, and Z.-X. Shen, Angle-resolved photoemission studies of quantum materials, *Rev. Mod. Phys.* **93**, 025006 (2021).
- [55] See Supplemental Material for details on experimental and computational methods, analysis on X-ray photoelectron spectroscopy (XPS), single crystal X-ray diffraction (XRD) and X-ray absorption spectroscopy (XAS) results, detailed analysis of the energy distribution curves and constant energy contours from ARPES experiment, additional DFT calculation results, and additional data for temperature and photon energy dependence ARPES measurements.
- [56] C. Jozwiak, J. A. Sobota, K. Gotlieb, A. F. Kemper, C. R. Rotundu, R. J. Birgeneau, Z. Hussain, D.-H. Lee, Z.-X. Shen, and A. Lanzara, Spin-polarized surface resonances accompanying topological surface state formation, *Nature Communications* **7**, 13143 (2016).
- [57] S. Moser, An experimentalist's guide to the matrix element in angle resolved photoemission, *Journal of Electron Spectroscopy and Related Phenomena* **214**, 29 (2017).
- [58] H. Park and I. Martin, DFT + DMFT study of the magnetic susceptibility and the correlated electronic structure in transition-metal intercalated nbs_2 , *Phys. Rev. B* **109**, 085110 (2024).
- [59] S. Mankovsky, S. Polesya, H. Ebert, and W. Bensch, Electronic and magnetic properties of $2h - \text{nbs}_2$ intercalated by 3d transition metals, *Phys. Rev. B* **94**, 184430 (2016).
- [60] D. N. Aristov, Indirect rkky interaction in any dimensionality, *Phys. Rev. B* **55**, 8064 (1997).
- [61] K.-T. Ko, K. Kim, S. B. Kim, H.-D. Kim, J.-Y. Kim, B. I. Min, J.-H. Park, F.-H. Chang, H.-J. Lin, A. Tanaka, and S.-W. Cheong, Rkky ferromagnetism with ising-like spin states in intercalated $\text{Fe}_{1/4}\text{TaS}_2$, *Phys. Rev. Lett.* **107**, 247201 (2011).
- [62] M. A. Ruderman and C. Kittel, Indirect exchange coupling of nuclear magnetic moments by conduction electrons, *Phys. Rev.* **96**, 99 (1954).
- [63] K. Fujita, C. K. Kim, I. Lee, J. Lee, M. H. Hamidian, I. A. Firmo, S. Mukhopadhyay, H. Eisaki, S. Uchida, M. J. Lawler, E.-A. Kim, and J. C. Davis, Simultaneous

- transitions in cuprate momentum-space topology and electronic symmetry breaking, *Science* **344**, 612 (2014).
- [64] Y. He, M. Hashimoto, D. Song, S.-D. Chen, J. He, I. M. Vishik, B. Moritz, D.-H. Lee, N. Nagaosa, J. Zaanen, T. P. Devereaux, Y. Yoshida, H. Eisaki, D. H. Lu, and Z.-X. Shen, Rapid change of superconductivity and electron-phonon coupling through critical doping in bi-2212, *Science* **362**, 62 (2018).
- [65] S.-D. Chen, M. Hashimoto, Y. He, D. Song, K.-J. Xu, J.-F. He, T. P. Devereaux, H. Eisaki, D.-H. Lu, J. Zaanen, and Z.-X. Shen, Incoherent strange metal sharply bounded by a critical doping in bi2212, *Science* **366**, 1099 (2019).
- [66] M. Yi, Y. Zhang, Z.-X. Shen, and D. Lu, Role of the orbital degree of freedom in iron-based superconductors, *npj Quantum Materials* **2**, 57 (2017).
- [67] Z. K. Liu, M. Yi, Y. Zhang, J. Hu, R. Yu, J.-X. Zhu, R.-H. He, Y. L. Chen, M. Hashimoto, R. G. Moore, S.-K. Mo, Z. Hussain, Q. Si, Z. Q. Mao, D. H. Lu, and Z.-X. Shen, Experimental observation of incoherent-coherent crossover and orbital-dependent band renormalization in iron chalcogenide superconductors, *Phys. Rev. B* **92**, 235138 (2015).
- [68] J. P. Perdew, K. Burke, and M. Ernzerhof, Generalized gradient approximation made simple, *Phys. Rev. Lett.* **77**, 3865 (1996).
- [69] A. I. Liechtenstein, V. I. Anisimov, and J. Zaanen, Density-functional theory and strong interactions: Orbital ordering in mott-hubbard insulators, *Phys. Rev. B* **52**, R5467 (1995).
- [70] G. Kresse and J. Furthmüller, Efficient iterative schemes for ab initio total-energy calculations using a plane-wave basis set, *Physical Review B* **54**, 11169 (1996).
- [71] S. F. Weber and J. B. Neaton, Origins of anisotropic transport in the electrically switchable antiferromagnet $\text{Fe}_{1/3}\text{NbS}_2$, *Phys. Rev. B* **103**, 214439 (2021).
- [72] Y. Saitoh, K. Kobayashi, A. Fujimori, Y. Yamamura, M. Koyano, T. Tsuji, and S. Katayama, Photoemission and core-level absorption spectroscopy of $\text{Fe}_{1/3}\text{NbS}_2$, *Journal of Electron Spectroscopy and Related Phenomena* **144-147**, 829 (2005), proceeding of the Fourteenth International Conference on Vacuum Ultraviolet Radiation Physics.
- [73] L. S. Xie, S. Husremović, O. Gonzalez, I. M. Craig, and D. K. Bediako, Structure and magnetism of iron- and chromium-intercalated niobium and tantalum disulfides, *Journal of the American Chemical Society* **144**, 9525 (2022), pMID: 35584537.
- [74] S. Kirchner, S. Paschen, Q. Chen, S. Wirth, D. Feng, J. D. Thompson, and Q. Si, Colloquium: Heavy-electron quantum criticality and single-particle spectroscopy, *Rev. Mod. Phys.* **92**, 011002 (2020).
- [75] J. Kondo, Resistance minimum in dilute magnetic alloys, *Progress of Theoretical Physics* **32**, 37 (1964).
- [76] P. Gegenwart, Q. Si, and F. Steglich, Quantum criticality in heavy-fermion metals, *Nature Physics* **4**, 186 (2008).
- [77] H. Prüser, P. E. Dargel, M. Bouhassoune, R. G. Ulbrich, T. Pruschke, S. Lounis, and M. Wenderoth, Interplay between the kondo effect and the ruderman-kittel-kasuya-yosida interaction, *Nature Communications* **5**, 5417 (2014).